Photodesorption and dissociation from a graphite surface

Contact *w.a.brown@sussex.ac.uk*

Daren J. Burke[1]

University College London
Department of Chemistry, 20 Gordon Street, London, WC1H 0AJ, UK.

[1]***Present address:*** *Department of Chemistry, University of Sussex, Falmer, Brighton, BN1 9QJ, UK.*

Wendy A. Brown[1]

University College London
Department of Chemistry, 20 Gordon Street, London, WC1H 0AJ, UK.

Introduction

The space between the stars, the interstellar medium (ISM), comprises clouds of gas and dust containing molecules, which play a crucial role in star formation. Studies show that gas-surface chemistry is essential to rationalise the abundance of many of these molecules. In the ISM, molecules freeze out on the cold (10 K) surfaces of grains, forming molecular ices consisting mainly of water, but also containing other species. Observations reveal the presence of more complex species (e.g. glycolaldehyde), indicative of the processing of these ices by exposure to ultra-violet (UV) light and low energy electrons.

Dust grains play a pivotal role in chemical processes in the ISM[1], opening up reaction pathways to atoms/molecules that accrete on the grains that are not available in the gas-phase[2]. In the cold regions of the ISM where star formation occurs, the role of the grains is two-fold. First they act as a third body, catalysing surface chemical reactions. Dust grains also provide a reservoir for the freeze-out of gaseous species to form molecular ices which undergo chemical and physical transformation *via* numerous routes, including UV irradiation.

The composition of interstellar ices depends on the environment. However, observations have established that these ices are dominated by H_2O (60-70%) with other abundant constituents including CO, CO_2, CH_3OH, CH_4 and NH_3[3]. These molecules are also precursors for the formation of complex molecular species (e.g. methyl formate and glycoaldehyde[4,5]) detected in gas and condensed phases.

Despite extensive laboratory simulations of interstellar ices[6], the role of UV irradiation in molecular formation and photodesorption has received considerably less attention[4,7]. This is surprising, since photochemistry is important in the formation of many complex organic species that cannot be formed in the gas-phase or via gas-grain reactions at the low temperatures and pressures of dense molecular clouds[8]. Similarly, the photochemical pathway is often overlooked in computational models, despite the fact that photoexcited states generated within ices or originating from the gas-phase, would provide sufficient energy to surpass otherwise insurmountable reaction energy barriers.

To date, most UV studies of ices have focused on resonant photon-induced processes within the ices, i.e. irradiating ices at wavelengths at which the parent molecules within the ice absorb light, leading to electronically excited states facilitating desorption or dissociation[4,7]. These experiments have been performed on insulators[7] and metals[4] and neglect substrate-mediated effects that lead to photodesorption and photodissociation[9]. Furthermore, these surfaces do not truly reflect the nature of dust grains, which are known to be silicaceous and carbonaceous in nature.

Methodology

Model interstellar ices of known thickness were grown on a highly oriented pyrolytic graphite (HOPG) sample, cooled to ~ 20 K to mimic low ISM temperatures. The low pressure conditions of the ISM were simulated by mounting the sample in an ultrahigh vacuum (UHV) apparatus, equipped with a pulse counting quadrupole mass spectrometer. A range of model interstellar ices grown on the HOPG substrate were investigated, including ices containing simple species such as CO_2, CH_3OH, CH_3CH_2OH, and HCO_2H, both with and without H_2O ice. Ices containing more complex organic species (glycolaldehyde and methyl formate) were also studied.

Samples were irradiated with a Nd^{3+}-YAG pumped dye laser at a repetition rate of 10 Hz. In order to study substrate-mediated photo-processes, samples were irradiated over the 217-224 nm wavelength range, where the chosen adsorbates are optically transparent. The laser beam was incident on the HOPG sample at an angle of 45°. The absolute laser power measured outside the window into the UHV chamber was of the order of 1–4.4 mW, depending on the incident wavelength, giving an energy of 0.1-0.44 mJ $pulse^{-1}$. Species desorbing from the ices were monitored with a pulse counting quadrupole mass spectrometer. Post-irradiation temperature programmed desorption (pi-TPD) spectra were also recorded, in order to characterise any photo-reactions that took place during laser irradiation.

Results and discussion

Initial experiments were performed in order to test and optimize the experimental set up. CO_2 containing model interstellar ices were chosen for optimisation, and Figure 1 shows a typical laser induced desorption (LID) profile for pure CO_2 ice adsorbed on HOPG, irradiated with 221 nm light at an energy of 0.23 mJ $pulse^{-1}$.

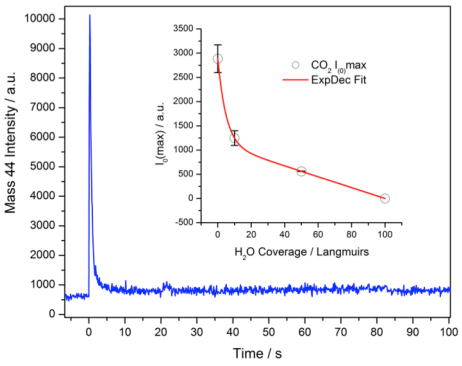

Figure 1: Typical LID signal for 5 L CO_2 adsorbed on HOPG irradiated with 221 nm light. The inset shows the initial peak height of the CO_2 LID signal as a function of the thickness of a pre-adsorbed H_2O spacer layer.

A very clear LID signal is observed for the parent molecule, however no evidence of photodissociation was observed (i.e. no CO or O desorption occurred). Data for pure CO_2 ice adsorbed on HOPG were recorded as a function of ice thickness (from 0.5 – 20 L) and laser wavelength. In order to prove that the observed LID was a substrate-mediated effect, experiments

were also performed where CO_2 was adsorbed on top of a H_2O spacer layer. The inset to Figure 1 shows the initial peak height of the CO_2 LID signal as a function of the thickness of the H_2O spacer layer. Clearly a thicker H_2O spacer layer inhibits CO_2 LID, indicating that the observed desorption is due to a substrate-mediated process. If desorption occurred due to direct absorption of light by the CO_2, the H_2O spacer layer would not affect the desorption. At this stage it is not possible to determine whether the substrate-mediated desorption is via an electron or phonon process.

Following the testing of the set up with CO_2, subsequent experiments were performed to investigate the LID and dissociation of a range of small organic molecules adsorbed on HOPG including CH_3OH, CH_3CH_2OH and HCO_2H. In all cases, data were recorded as a function of ice thickness for pure ices and for ice mixtures consisting of the molecule of interest co-deposited with H_2O in a binary ice. In all cases LID was observed, with signal profiles recorded similar to those observed for CO_2. As well as looking for desorption of the intact molecule, the desorption of possible dissociation fragments of each of the adsorbed molecules was also monitored. In addition, pi-TPD was performed to identify any dissociation/reaction products. For HCO_2H, only desorption of the parent molecule was observed in both LID and post-irradiation TPD. The signal intensity was also weakest for HCO_2H. However, for CH_3OH and CH_3CH_2OH, laser induced dissociation/reaction was also seen.

Figure 2A shows a typical LID profile for CH_3OH desorbing from a mixed CH_3OH:H_2O ice (2 L) irradiated with 223 nm radiation at 0.23 mJ pulse^{-1}.

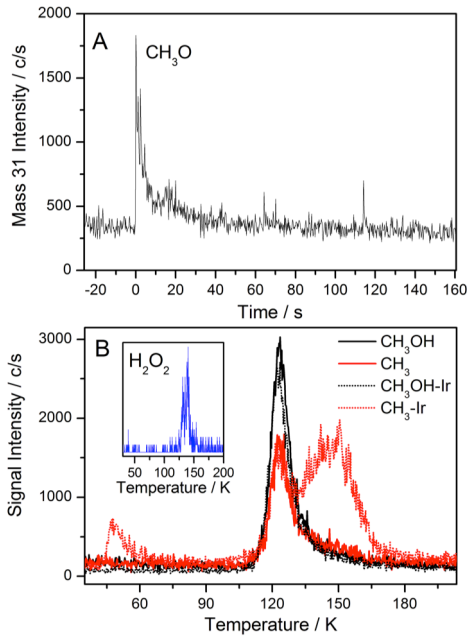

Figure 2: A shows a typical LID signal for CH_3OH desorbing from a mixed CH_3OH:H_2O ice. B shows post-irradiation TPD of masses 31 (CH_3O – the main fragment of CH_3OH) and mass 15 (CH_3). The inset to B shows the desorption of H_2O_2 from the post-irradiated CH_3OH:H_2O ice.

As well as mass 31 (the main cracking fragment of CH_3OH), LID of mass 15 (CH_3) is also observed. Since mass 15 is also a cracking fragment of CH_3OH in the mass spectrometer, pi-TPD were recorded to determine the origin of the observed CH_3 desorption. Figure 2B shows the results of pi-TPD for CH_3OH adsorbed on HOPG. The figure shows TPD for irradiated (solid lines) and non-irradiated (dotted lines) ices. Clearly there is an additional desorption peak for mass 15 from the irradiated ices, that is not observed for non-irradiated ices. This peak is not associated with mass 31 desorption, and cannot therefore be attributed to the cracking of CH_3OH in the mass spectrometer.

This result is very interesting as it implies that dissociation of CH_3OH occurs upon irradiation of the ice. The same result is observed for mixed CH_3OH:H_2O ices adsorbed on HOPG. To further investigate the CH_3OH dissociation, H_2O_2 desorption was monitored in the pi-TPD. The inset to Figure 2B shows the TPD signal observed for H_2O_2 desorption from a mixed CH_3OH:H_2O ice, following laser irradiation. The observation of H_2O_2 in the TPD indicates the formation of the OH radical on the surface (the other fragment of CH_3OH dissociation), which then desorbs recombinatively to give H_2O_2 in the TPD spectrum. The observed UV induced dissociation of CH_3OH is potentially very significant with respect to interstellar chemistry, as it provides a pathway by which CH_3 and OH can be produced to then go on to react to form other species. Further investigations are required in order to determine the exact nature of this laser induced dissociation process.

The final series of experiments involved laser irradiation of the more complex organic molecules methyl formate (MeF) and glycolaldehyde (GA). In both cases LID was seen, but no dissociation induced by laser irradiation could be detected. Data were recorded for pure ices and for mixtures of GA/MeF and H_2O. For MeF, very interesting effects were observed when MeF:H_2O mixtures were irradiated at 223 nm as seen in Figure 3.

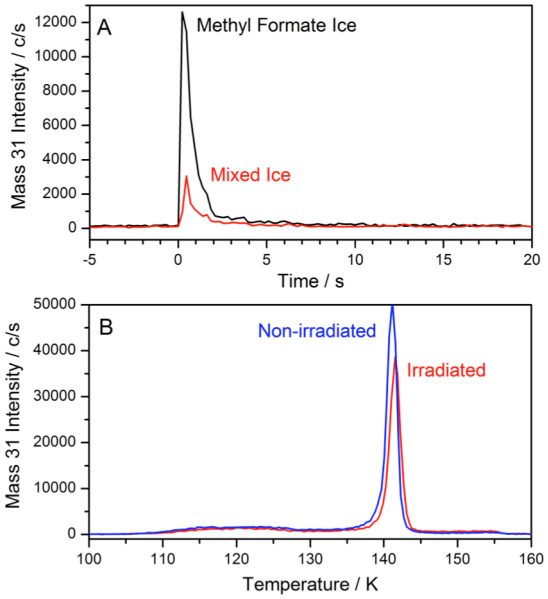

Figure 3: A shows a comparison of the LID signal following irradiation of a mixed MeF:H_2O ice (red trace) and irradiation of the same amount of pure MeF ice (black trace). B shows post-irradiation TPD spectra of mixed MeF:H_2O ices (red line) compared with TPD spectra for an equivalent unirradiated ice (blue line).

Figure 3A shows LID traces for 8 L pure MeF ice (black trace) and for a mixed ice containing 8 L of MeF codeposited with 16 L of H_2O ice (red trace). Clearly the presence of H_2O in the mixed ice severely inhibits the LID of MeF. This is an important observation with respect to the ISM, since MeF is only found in the presence of large quantities of H_2O ice. Whilst H_2O ice clearly inhibits the LID of MeF, Figure 3B shows that there is still a significant effect of laser irradiation on a mixed MeF:H_2O ice. This figure shows a comparison of TPD spectra for irradiated (red line) and non-irradiated (blue line) mixed MeF:H_2O ices. For the irradiated ices, there is considerably less desorption of intact MeF, implying that the laser irradiation has given rise to desorption or dissociation of the MeF ice.

Conclusions

Laser irradiation of a range of model ices over the 217-224 nm range has shown clear evidence of LID for a range of astrophysically relevant molecules. For all molecules studied, LID was observed. Studies of CO_2 adsorbed on HOPG confirm that the observed LID is a substrate-mediated effect. Further investigations are necessary in order to determine whether the effects observed are phonon or electron mediated. LID was also observed for a range of simple and more complex organic molecules. For CH_3OH, additional laser induced dissociation was observed, with evidence for both CH_3 and OH fragments being seen, in addition to H_2O_2 formation during pi-TPD. Studies of MeF have also shown that the presence of H_2O has a significant effect on the LID of MeF. This result is very important for the ISM, since interstellar ices are comprised mainly of H_2O.

Acknowledgements

We thank the Leverhulme Trust for funding for DJB. WAB acknowledges support from the European Community's Seventh Framework Programme FP7/2007-2013 under grant agreement no. 238258. Ian Clark (laser loan pool manager) and Ben Agate (Photonics UK) are thanked with their help in optimising the optical set up.

References

1. D.A. Williams, in *Dust and Chemistry in Astronomy*, eds. T.J. Millar and D.A. Williams, Institute of Physics Publishing, Bristol, Edition, 1993; D.C.B. Whittet, *Dust in the Galactic Environment*, Institute of Physics Publishing, Bristol, 2003.
2. B.T. Draine, *Annu. Rev. Astron. Astrophys.*, 2003, **41**, 241.
3. E.L. Gibb, et al., *ApJ*, 2000, **536**, 347.
4. K.I. Oberg, R.T. Garrod, E.F. van Dishoeck, H. Linnartz, *Astron. Astrophys.*, 2009, **504**, 891.
5. C J. Bennett, R.I. Kaiser, *ApJ*, 2007, **661**, 899.
6. D.J. Burke, W.A. Brown, *PCCP*, 2010, **12**, 5947.
7. L.J Allamandola, S.A. Sandford, G.J. Valero, *Icarus*, 1988, **76**, 225.
8. W.H. Sorrell, *ApJ*, 2001, **555**, L129.
9. X-L. Zhou, X-Y. Zhu, J.M. White, *Surf. Sci. Rep.* 1991, **13,** 1.

The role of a heme pocket lysine residue during the geminate recombination of NO in the hemoprotein cytochrome c'.

Contact *Derren.heyes@manchester.ac.uk*

Henry J. Russell

Manchester Institute of Biotechnology, University of Manchester, 131 Princess Street, Manchester M1 7DN, UK

Nigel S. Scrutton

Manchester Institute of Biotechnology, University of Manchester, 131 Princess Street, Manchester M1 7DN, UK

Derren J. Heyes

Manchester Institute of Biotechnology, University of Manchester, 131 Princess Street, Manchester M1 7DN, UK

Samantha J. O. Hardman

Manchester Institute of Biotechnology, University of Manchester, 131 Princess Street, Manchester M1 7DN, UK

Sam Hay

Manchester Institute of Biotechnology, University of Manchester, 131 Princess Street, Manchester M1 7DN, UK

Michael A. Hough

School of Biological Sciences, University of Essex, Wivenhoe Park, Colchester, Essex, CO4 3SQ, UK

Greg M. Greetham

Central Laser Facility, STFC Rutherford Appleton Laboratory, Harwell Campus, Didcot, UK

Mike Towrie

Central Laser Facility, STFC Rutherford Appleton Laboratory, Harwell Campus, Didcot, UK

Introduction

Hemoproteins are implicated in a range of metabolic processes including electron transport, gas transport, catalysis, and sensory pathways [1]. The functions of these proteins are often regulated by intracellular binding of the diatomic molecules nitric oxide (NO), carbon monoxide (CO), or molecular oxygen (O_2). Due to their respective electron distributions, these molecules bind to free heme with affinities NO >> CO >> O_2, and as a result hemoproteins have developed sophisticated structural properties to discriminate between these markedly similar gases [2]. The protein matrix is proposed to play an important role in ligand-heme stability and dissociation [3].

One such example, cytochrome c', has proven to be an excellent model system for understanding how precise structural arrangements modulate the affinity of the heme cofactor for these diatomic gases in hemoproteins. Cytochrome c' is present in a variety of nitrogen-fixing, denitrifying and photosynthetic bacteria. Physiologically cytochrome c' is implicated in NO transport and reduction of intracellular NO toxicity [4-7]. A great deal of recent *in vitro* work has focussed on cytochrome c' from *Alcaligenes xylosoxidans* (*Ax*Cytcp) in part due to its spectroscopic similarities to soluble guanylate cyclase which, upon binding NO, regulates a number of signal cascades in higher organisms including vasodilation and neurotransmission [1]. In the absence of a crystal structure for soluble guanylate cyclase, *Ax*Cytcp has been utilised as a model system in order to increase the mechanistic understanding of soluble guanylate cyclase [8].

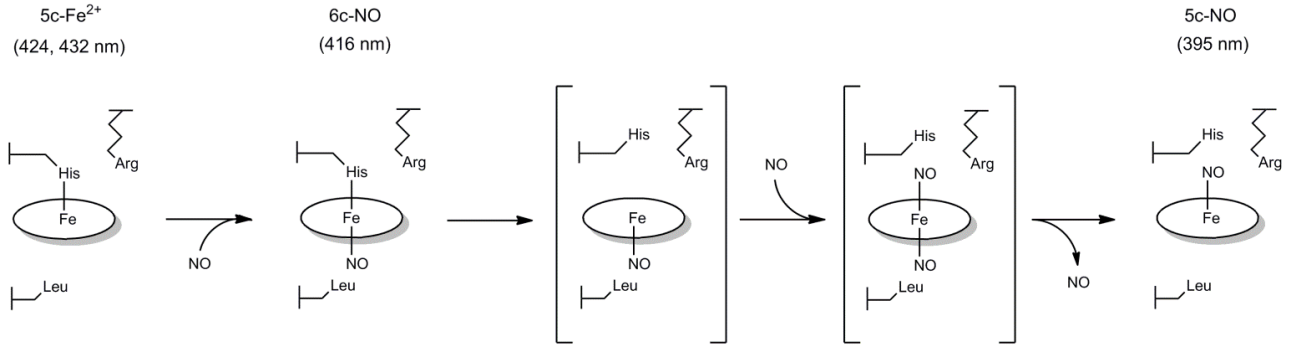

Scheme 1. The currently proposed distal-to-proximal mechanism of NO binding in *Ax*Cytcp adapted from Ref. 9. Initially, an NO molecule binds to the hydrophobic distal face forming a 6c-NO species.. The Fe-His bond is then cleaved, allowing a second NO to bind on the proximal face forming a putative dinitrosyl intermediate. Finally, the distal NO detaches, leaving a proximally bound, 5c-NO species. Hypothesized, short-lived intermediates are denoted by square brackets. Leu 16 is thought to be necessary to weaken the Fe-His bond to form the 5c-NO species.

Unlike the majority of hemoproteins, *Ax*Cytcp forms a proximal 5c-NO adduct via the mechanism outlined in Scheme 1, which has been postulated based on a number of spectroscopic and crystallographic studies [9-13]. Initially, NO binds distally to form a 6c-NO intermediate, the lifetime of which is extended by a proximal arginine residue [9]. This initial binding event weakens the proximal His-Fe bond due to the repulsive *trans* effect of NO, allowing the displacement of the His-Fe bond by a second NO, forming a distal pocket environment, mediated by a leucine residue, the distal NO is repelled by the proximal NO, leaving the final proximal 5c-NO adduct. In contrast, CO forms a distal 6c-CO adduct, apparently lacking the ability to sufficiently weaken the His-Fe bond [10], while O_2 is completely excluded from the heme pocket [14].

Previous studies have shown that this discrimination between ligands is mediated largely by the hydrophobic leucine [14, 15]. When this residue is mutated to alanine the distally bound NO fails to weaken the His-Fe bond sufficiently and remains in the 6c-NO position [14]. When CO is bound to this mutant it demonstrates the highest affinity ever reported in a hemoprotein [15], and possibly most significantly, this mutant lacks the ability to exclude O_2 from the heme binding site [14]. In the as-isolated form *Ax*Cytcp has been shown by transient absorption (TA) and resonance Raman measurements to bind 5c-NO in a highly controlled environment [16, 17]. This is demonstrated by the high proportion of geminate recombination after excitation (~ 99 %) on a fast timescale (7 ps) [16]. For the small proportion that undergoes His rebinding, this "kinetic trap" prevents the rebinding of NO, which instead undergoes solvent rebinding as shown by laser-flash photolysis [18]. These findings highlight the control the proximal *Ax*Cytcp structure has in minimising NO escape.

A useful tool in monitoring the contribution of heme pocket residues in these processes is by ultrafast spectroscopy techniques using mutated versions of proteins [3]. In this work we have explored the role of the distal leucine in maintaining the stability of the heme binding pocket by studying the geminate recombination of NO to a L16G mutant using time-resolved spectroscopy in the infrared (TRIR) and in the UV-vis region (transient absorption - TA). These measurements have provided an insight into the structural events during geminate recombination and have allowed a comparative analysis between 5c-NO and 6c-NO binding.

MATERIALS AND METHODS

AxCytcp preparation. Wild-type and L16G *Ax*Cytcp were overexpressed and purified as previously described [15, 19]. WT samples were isolated in MES buffer, pH 6.0 in the ferric form and purity was estimated by SDS-polyacrylamide gel electrophoresis and UV-vis spectroscopy, with the concentration estimated using ε_{400} = 80,000 $M^{-1}cm^{-1}$ [20]. Samples were reduced using an excess of sodium dithionite (~ 10 mM) in an anaerobic glove box (Belle Technology) and passed down a desalting column (Centri Pure P25 – EMP Biotech) equilibrated with anaerobic 50 mM CHES buffer, pH 8.9 (D_2O for infrared measurements adjusted to pD 8.9) to remove excess reductant. The concentration of the ferrous sample was estimated using ε_{426} = 97,000 $M^{-1}cm^{-1}$ [20]. The L16G variant was isolated with CO bound to the heme distal face as previously reported [16]. This ligand was removed by incubating with an excess of potassium ferricyanide (500 mM) for one hour at room temperature under anaerobic conditions. Excess oxidant was removed by passage down a desalting column equilibrated with anaerobic 50 mM MES buffer, pH 6.0. The sample was then reduced using an excess of sodium dithionite (~ 10 mM) and passed down a desalting column pre-equilibrated with anaerobic 50 mM CHES buffer, pH 8.9 (D_2O for infrared measurements adjusted to pD 8.9). The concentration was estimated using ε_{420} = 80,000 $M^{-1}cm^{-1}$.

TA measurements. A Ti:sapphire amplifier (a hybrid Coherent Legend Elite-F-HE) was pumped by a Q-switched Nd:YLF laser (Positive Light Evolution-30) and seeded by a Ti:sapphire laser (Spectra-Physics Mai Tai). The amplifier has an output wavelength of 800 nm, a 1 kHz repetition rate, and a 120 fs pulse duration. This beam is then split, with part of the output used to produce tuneable radiation in the range 250 to 1000 nm *via* a non-collinear optical parametric amplifier (Light Conversion TOPAS-White). Another fraction of the amplifier output is used to pump Helios and Eos (Ultrafast Systems LLC) broadband pump-probe transient absorption spectrometers, with instrument response functions of around 170 fs and 500 ps, respectively. In all cases, samples were excited at 532 nm with 0.5 – 1 µJ power and a beam diameter of ~ 200 µm. Absorption changes were monitored between 350 – 700 nm at time delays between 100 fs – 3 ns after excitation for Helios experiments and from 0.5 ns – 400 µs for Eos experiments. Reduced samples were added to 2 mm pathlength quartz cuvettes and adjusted to a concentration such that the Soret band had an absorbance reading of ~ 0.7. A superseal was then attached to the cuvette entrance inside an anaerobic glovebox and NO gas bubbled into the cuvette until the spectrum resembled the respective NO-bound profile. Samples were stirred to avoid photobleaching.

TRIR spectroscopy. Time resolved infrared measurements were carried out using an ultrafast TRIR experimental setup described previously [21], with a 10 kHz repetition rate and 100 fs time resolution. *Ax*Cytcp samples were prepared to a ferrous concentration of ~ 2 mM, then either analyzed without NO bound or incubated with 3.5 mg spermine NONOate (Tocris bioscience – Cat No. 1135) for 4 hrs at room temperature to allow NO binding (~ 25 mM of NO liberated). Samples were then added to an anaerobic cell with CaF_2 windows and a 75 µm spacer, which was rastered to avoid sample damage. For all samples an excitation wavelength of 532 nm was used with 1 µJ pulse power and a beam diameter of ~ 150 µm set at the magic angle with respect to the IR probe beam. Spectra were measured at time delays ranging between 500 fs and 1 ns. Difference spectra were generated relative to the ground state in the spectral window 1300-1800 cm^{-1}. This was measured using two 128 pixel detectors with a spectral resolution of approximately 3 cm^{-1} per pixel. Pixel to wavenumber calibration was calculated as previously shown [22].

Global fitting. Kinetic analyses were carried out using Origin 8.5 software. Five spectral positions of significant absorption change in the TA and TRIR were selected and fit with shared lifetime values using the global fitting option.

RESULTS AND DISCUSSION

Wild-type AxCytcp. The UV-vis (figure 1) and IR (figure 2) ground state absorption spectra of reduced and NO-bound wtCcp are shown to highlight the spectral regions of interest. For both TA and TRIR experiments a similar excitation wavelength (532 nm), laser power (1 µJ) and beam diameter (~ 150 µm) was used, therefore the respective spectral and kinetic data can be directly compared. The TA difference spectra (figure 3A) show a ground state bleach at 393 nm and an equivalent transient feature centered at 420 nm, both of which decay almost completely to the ground state over ~ 100 ps. The minimal signal remaining after 100 ps (~ 5 % of the initial signal remaining at 396 nm) has previously been assigned to the 5c-His species formed upon NO escape to the surrounding solvent [17].

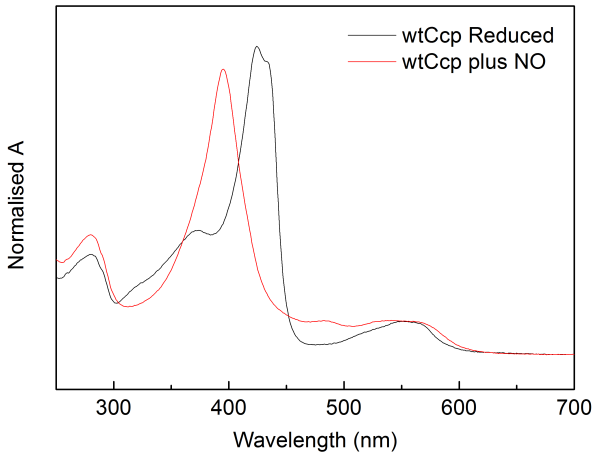

Figure 1. UV-vis spectra for reduced and NO-bound samples of wtCcp normalised to A_{700}. When reduced, wtCcp exhibits a split Soret band with peak positions 424 and 432 nm which shifts to a single Soret upon NO-binding centered at 395 nm.

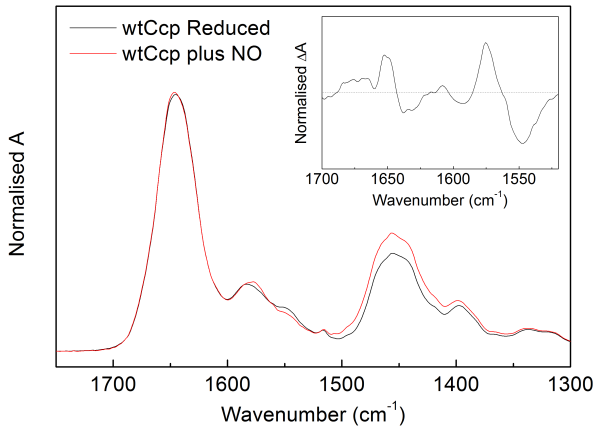

Figure 2. Infrared spectra for reduced (black trace) and NO-bound (red trace) wtCcp with difference spectra (NO-bound minus reduced) inset. The spectra are normalised to frequencies of no signal change. In all cases the spectra illustrate characteristic protein spectral structure, with an amide I band centered at 1645 cm^{-1} and amide II centered at 1455 cm^{-1}. The amide II band appears to broadly increase upon addition of NO, while the amide I stretch shows more subtle changes. There are a number of increases which complement existing IR assignments for NO binding to cytochrome c' [1].

The equivalent TRIR difference spectra (figure 3B) reveal a number of features, the most prominent of which include signal bleaches at 1656, 1678 (shoulder) and 1577 cm^{-1}, and transient features at 1717, 1745 (shoulder), 1637, 1602 and 1556 cm^{-1}. There are also a number of less pronounced features from 1300-1500 cm^{-1}. The 1656 cm^{-1} bleach has previously been assigned to the 5c-NO species [12] and therefore provides the opportunity to directly monitor NO geminate recombination. The overall TRIR difference spectra suggest that the vast majority of photolysed NO in wtCcp undergoes geminate recombination on a fast timescale, as previously suggested [16]. The transient features at frequencies higher than 1700 cm^{-1} warrant discussion as these signals reside outside of the amide I band. This increase in IR absorbance could correspond to the emergence of carbonyl (C=O) groups following excitation, as these groups give strong absorbance between 1670 – 1820 cm^{-1} due to a stretching motion [23]. According to the wtCcp NO-bound crystal structure [9], His120 is hydrogen bonded to an aspartate residue (Asp121) in contrast with the reduced structure. Therefore, following excitation of NO, this His-Asp H-bond could potentially cleave, allowing competition between the His and NO for proximal binding, and temporarily reveal the carbonyl group of Asp121.

In order to determine which spectral features correspond to heme vibrations following excitation, control TRIR experiments were performed using reduced wtCcp in the absence of NO. As expected, the difference spectra for reduced wtCcp exhibits a markedly reduced 1656 cm^{-1} band, but retains a number of other spectral features (figure 4). When compared directly, the TRIR data for wtCcp in the presence and absence of NO have a number of common spectral features, particularly in the fingerprint region of 1300-1500 cm^{-1}. The only noteworthy differences are transient features at 1637 and 1717 cm^{-1}, and the 1656 cm^{-1} bleach with a shoulder at 1676 cm^{-1}. We therefore suggest that the signals below 1600 cm^{-1} report on excitation of the heme and structural changes in coordinating protein residues [24]. It is noteworthy that the 1573 cm^{-1} band has been previously suggested to report on either the histidine or arginine residue during NO binding [12]. Our data make either improbable considering this signal bleach is present in the wtCcp with NO bound (histidine displaced).

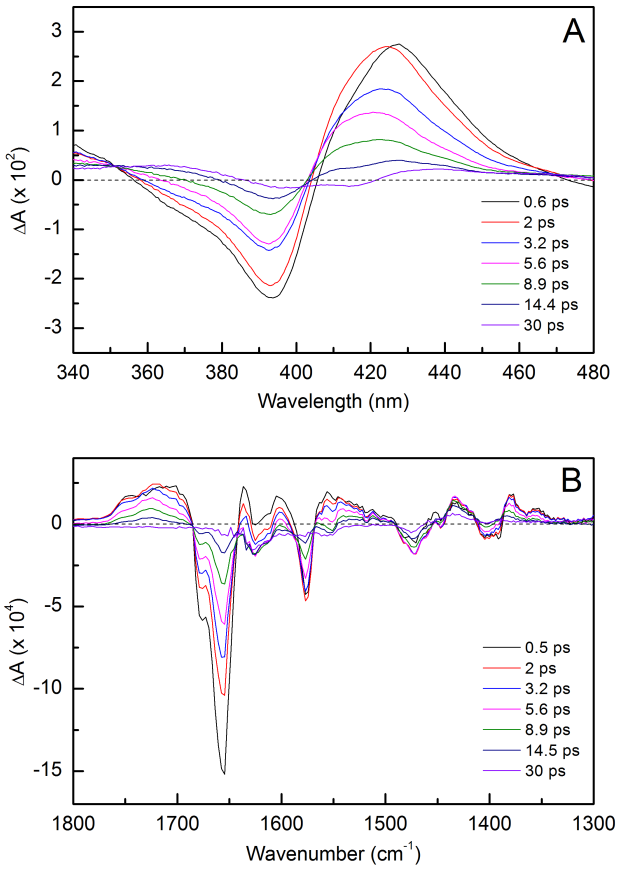

Figure 3. TA (A) and TRIR (B) difference spectra relative to the ground state for wtCcp following photolysis of the bound NO by laser excitation. TA difference spectra from 0.5 – 30 ps illustrate a ground state bleach at 393 nm and an equivalent transient at 420 nm which return to the ground state almost completely after 30 ps. The most noteworthy feature in the TRIR difference spectra is the 1656 cm^{-1} signal bleach corresponding to cleavage of the 5c-NO bond.

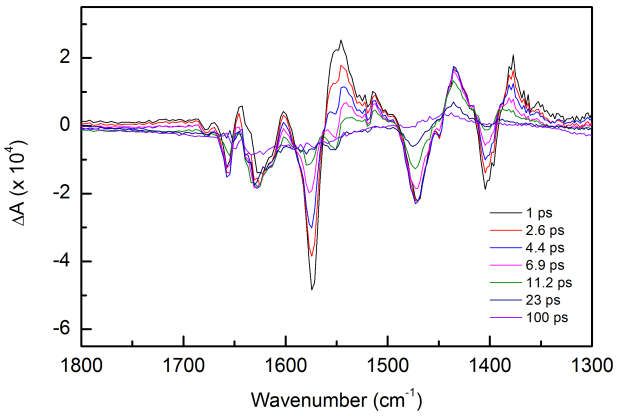

Figure 4. Reduced wtCcp TRIR difference spectra relative to the ground state between 1-100 ps after excitation. This illustrates signal bleaches at 1575, 1471 and 1405 cm^{-1}, and transient features at 1377, 1436 and 1546 cm^{-1}, with a small but markedly reduced signal bleach at 1656 cm^{-1} which corresponds to a lack of 5c-NO in this species.

Kinetics for the TA and TRIR spectra were calculated by globally fitting the signal decays at five distinct wavelength or wavenumber values, using shared lifetimes and a non-linear least squared fitting model (UV-vis global fitting shown in Figures 5). This returned three spectral components as opposed

to the previously reported two (Table 1) [17], the ~ 7 ps component, which corresponds to geminate recombination of NO, and the ~ 100 ps component corresponding to His rebinding are also observed in our data. The variation in τ_3 between the TA experiments is likely due to the low amplitude of this lifetime component (with the consequent large error). The TRIR experiments were used principally to determine vibrational changes during geminate recombination (initial 10 ps after excitation), therefore very few data points at longer times were acquired, which explains the poorly resolved τ_3 value for these data. The additional fast component (τ_1) is of unknown identity, since for the majority of NO-binding hemoproteins geminate recombination occurs monoexponentially over ~ 7 ps [3] However, an exception was demonstrated during a study of myoglobin NO binding, which reported a fast 1 ps rebinding event not observed with most other systems [26]. The NO signal bleach in the TRIR (1656 cm^{-1}) suggests that this fast component also corresponds to NO rebinding, since on these timescales the signal amplitude is returning to the ground state. The first solved crystal structure of wtCcp suggested that multiple conformers of the NO–heme complex exist, and therefore this component could be fast recombination of a proportion of NO in a different conformation [9]. However, this hypothesis must be treated with caution since a later crystal structure reported only one orientation of bound NO [10]. It is noteworthy that this fast component is unlikely to correspond to a vibrationally excited NO rebinding to the heme, as no obvious bandshifts are observed, particularly of the 1656 cm^{-1} feature.

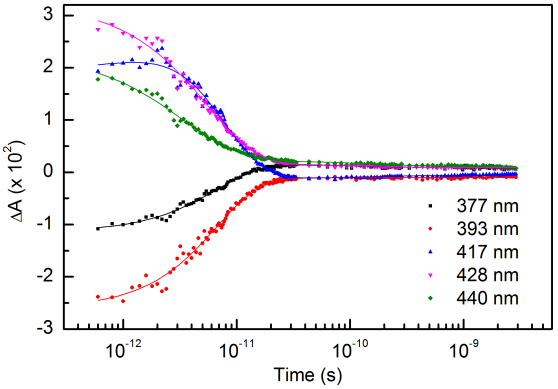

Figure 5. wtCcp TA absorption at five distinct wavelengths fit to the sum of three exponentials using shared lifetimes and a non-linear least squared fitting model.

Table 1. Kinetic lifetimes of wtCcp from TA and TRIR data (figure 3A and 3B respectively) when globally fit to the sum of three exponentials. The τ_3 value in the TRIR was poorly resolved due to the low quantity of data points acquired beyond 20 ps. These values are compared to existing kinetic data from Ref. 17.

	TA	TRIR	Literature TA[17]
τ_1	2.19 ± 0.18 ps	1.31 ± 0.16 ps	-
τ_2	5.65 ± 0.15 ps	6.13 ± 0.29 ps	7 ± 0.5 ps
τ_3	204 ± 56 ps	> 20 ps	100 ± 10 ps

L16G AxCytcp. Previous studies have shown that L16 variants of Ccp bind NO on the distal face in a 6c-NO mode (with the proximal histidine still attached) [15], without proceeding to a proximal binding mode. Consequently, the L16G variant has been used to probe the geminate recombination of NO to the distal face of the heme cofactor. The UV-vis ground state absorption spectra of L16G Ccp reveal a sharp, new peak at 416 nm, which corresponds to the formation of a 6c-NO species (figure 6). In the IR region there is an increase at 1630 cm^{-1} and corresponding decrease at 1655 cm^{-1} upon formation of the 6c-NO species for L16G (figure 7). TA and TRIR difference spectra for the geminate recombination of NO to the L16G variant are shown in figure 8, both of which are distinct from the wtCcp spectra. The TA difference spectra exhibits a ground state bleach centered at 416 nm, corresponding to the ground state UV-vis absorption spectrum of 6c-NO, and transient features at 370 and 435 nm that decay to the ground state within 1 ns. The TRIR data show obvious spectral differences to wtCcp (figure 9), with the ground state bleach shifted from 1656 to 1629 cm^{-1}. This is in agreement with an earlier assignment of a 6c-NO species at this position [12], and therefore likely represents the release of NO from the 6c distal binding site, presumably leaving a 5c-His intermediate. The broad transient feature at 1717 cm^{-1}, which was present in the wtCcp sample, is missing in the L16G sample. This complements our hypothesis stating that the > 1700 cm^{-1} features report on the Asp121 carbonyl group, since this residue is no longer hydrogen bonded to His120 when NO is bound in the 6c distal position. It appears from the TRIR difference spectra that the ground state molecule is fully reformed after ~ 1 ns, with no escape of NO to the bulk solvent. This is not surprising as any NO released from the distal pocket into solvent could simply rebind in the absence of any kinetic trap mechanism (as proposed with wtCcp).

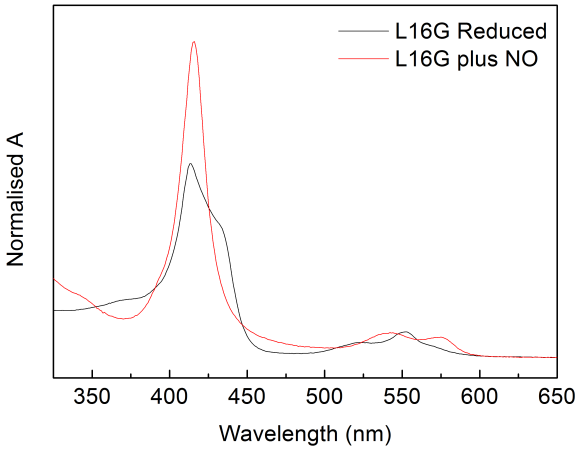

Figure 6. UV-vis spectra for reduced and NO-bound samples of L16G normalised to A_{700}. When reduced, L16G exhibits a split Soret band with peak positions 416 and 432 nm which shifts to a single Soret upon NO-binding centered at 416 nm.

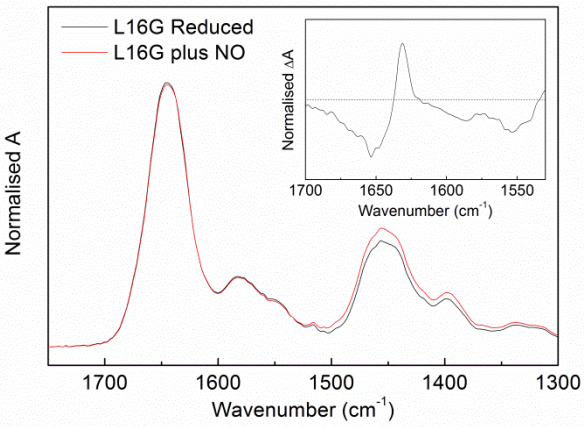

Figure 7. Infrared spectra for reduced (black trace) and NO-bound (red trace) L16G with difference spectra (NO-bound minus reduced) inset. The spectra are normalised to frequencies of no signal change. The difference spectra illustrate an increase at 1630 cm^{-1} and equivalent decrease at 1655 cm^{-1} relating to an increase in 6c-NO species.

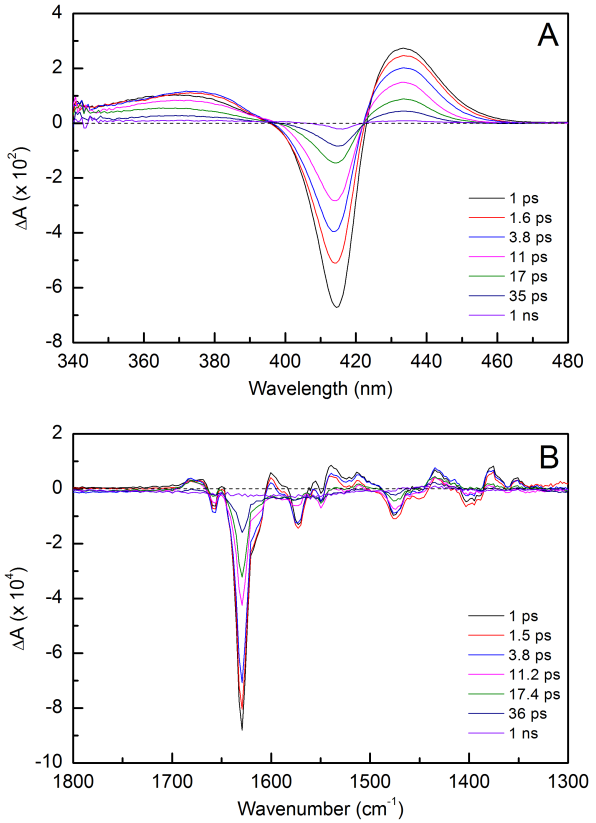

Figure 8. L16G TA (A) and TRIR (B) difference spectra at equivalent time points following excitation between 1 ps and 1 ns. TA difference spectra exhibit a ground state bleach at 416 nm, in accordance with the ground state spectrum and transients at 370 and 435 nm. The TRIR illustrates a signal bleach at 1629 cm^{-1} which likely corresponds to loss of a 6c-NO species, whilst the majority of other spectral features are also present in the wtCcp TRIR spectra.

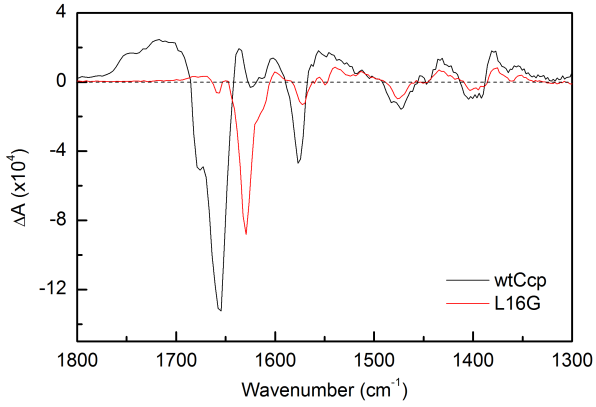

Figure 9. Comparison of TRIR 1 ps difference spectra for wtCcp and L16G. Broadly identical spectral features are observed from 1300-1600 cm^{-1}, which most likely correspond to heme vibrations. The major spectral differences are the shift in bleach from 1656 to 1629 cm^{-1} which correlates to 5c-NO and 6c-NO binding respectively, and the loss of transient signal at 1717 cm^{-1}.

L16G TA and TRIR data were globally fitted to the sum of two exponentials in all cases. However, lifetime values extracted from these data appeared to be affected by both the concentration of NO in solution and the concentration of protein studied. The lifetimes extracted from data with varying protein and NO concentrations in TA and TRIR experiments are presented in Table 2 and show that with an increasing NO:protein ratio, the lifetime values for both exponentials decreased, indicating they are both second order. This concentration-dependence could be due to the accessibility of the distal pocket to solvent, which influences the rate of rebinding after excitation. This makes direct comparison between TA and TRIR data particularly difficult for this variant, but the qualitative analysis of these datasets remains a useful feature.

Table 2. The influence of NO and protein concentration on the exponential fit of L16G.

Experiment	[L16G]	[NO]	τ_1 (ps)	τ_2 (ps)
TA	50 µM	100 % (2 mM)	1.21 ± 0.21	15.54 ± 0.89
TA	50 µM	NONOate – low	3.85 ± 0.17	18.45 ± 0.42
TRIR	2 mM	NONOate – low	5.85 ± 0.59	24.6 ± 2.2

Conclusions

The ability of Ccp to bind NO and CO on opposite faces of the heme, and the availability of variants where ligand binding is radically altered, renders it an excellent model system for understanding how precise structural arrangements modulate the affinity of the heme cofactor for these diatomic gases in hemoproteins. We have shown the importance of heme pocket architecture in the geminate recombination of NO. The removal of a single distal residue (L16) allows NO to bind to the distal face of the heme cofactor, creating a 6c-NO species. We have highlighted the kinetic and spectral (UV-vis and IR) differences for the geminate recombination of NO to either side of the heme cofactor and have shown that there is no escape of NO to the bulk solvent in an L16G variant. This work illustrates the importance of heme pocket architecture in modulating the control over heme-ligand reactivity and could have significant implications for other gas-binding proteins.

Acknowledgements

This work was supported by the Biotechnology and Biological Sciences Research Council (BBSRC). S.H. is a BBSRC David Phillips Fellow. N.S.S. is a Wolfson Merit Award holder and holds an Engineering and Physical Sciences Research Council (EPSRC) Established Career Fellowship. The TRIR measurements were carried out through program access support of the Science and Technology Facilities Council.

References

1. Gilles-Gonzalez, M.; Gonzalez, G., Heme-based sensors: defining characteristics, recent developments, and regulatory hypotheses. *J. Inorg. Biochem.* **2005,** 99, 1-22.
2. Tsai, A.; Martin, E.; Berka, V.; Olson, J. S., How Do Heme-Protein Sensors Exclude Oxygen? Lessons Learned from Cytochrome c', Nostoc puntiforme Heme Nitric Oxide/Oxygen-Binding Domain, and Soluble Guanylyl Cyclase. *Antioxidants and Redox Signaling* **2012,** 17, 1246-1262.
3. Vos, M., Ultrafast dynamics of ligands within heme proteins. *Biochim. Biophys. Acta* **2008,** 1777, 15-31.
4. Cross, R.; Aish, J.; Paston, S. J.; Poole, R. K.; Moir, J. W. B., Cytochrome c′ from Rhodobacter capsulatus Confers Increased Resistance to Nitric Oxide. *J. Bacteriol.* **2000,** 182, 1442-1447.
5. Cross, R.; Lloyd, D.; Poole, R. K.; Moir, J. W. B., Enzymatic Removal of Nitric Oxide Catalyzed by Cytochrome c′ in Rhodobacter capsulatus. *J. Bacteriol.* **2001,** 183, 3050-3054.
6. Mayburd, A. L.; Kassner, R. J., Mechanism and Biological Role of Nitric Oxide Binding to Cytochrome c‘. *Biochemistry* **2002,** 41, 11582-11591.

7. Choi, P. S.; Grigoryants, V. M.; Abruna, H. D.; Scholes, C. P.; Shapleigh, J. P., Regulation and Function of Cytochrome c′ in Rhodobacter sphaeroides. *J. Bacteriol.* **2005,** 187, 4077-4085.

8. Martin, E.; Berka, V.; Sharina, I.; Tsai, A. L., Mechanism of NO binding to soluble guanylyl cyclase: implication for the second NO binding to the heme proximal site. *Biochemistry* **2012,** 51, 2737-2746.

9. Hough, M. A.; Antonyuk, S. V.; Barbieri, S.; Rustage, N.; McKay, A. L.; Servid, A. E.; Eady, R. R.; Andrew, C. R.; Hasnain, S. S., Distal-to-Proximal NO Conversion in Hemoproteins: The Role of the Proximal Pocket. *J. Mol. Biol.* **2011,** 405, 395-409.

10. Lawson, D. M.; Stevenson, C. E. M.; Andrew, C. R.; Eady, R. R., Unprecedented proximal binding of nitric oxide to heme: implications for guanylate cyclase. *EMBO J.* **2000,** 19, 5661-5671.

11. Lawson, D. M.; Stevenson, C. E. M.; Andrew, C. R.; George, S. J.; Eady, R. R., A two-faced molecule offers NO explanation: the proximal binding of nitric oxide to haem. *Biochem. Soc. Trans.* **2003,** 31, 553-557.

12. George, S. J.; Andrew, C. R.; Lawson, D. M.; Thorneley, R. N.; Eady, R. R., Stopped-flow Infrared Spectroscopy Reveals a Six-Coordinate Intermediate in the Formation of the Proximally Bound Five-Coordinate NO adduct of Cytochrome c'. *J. Am. Chem. Soc.* **2001,** 123, 9683-9684.

13. Andrew, C. R.; George, S. J.; Lawson, D. M.; Eady, R. R., Six- to Five-Coordinate Heme-Nitrosyl Conversion in Cytochrome c' and Its Relevance to Guanylate Cyclase. *Biochemistry* **2002,** 41, 2353-2360.

14. Garton, E. M.; Pixton, D. A.; Peterson, C. A.; Eady, R. R.; Hasnain, S. S.; Andrew, C. R., A Distal Pocket Leu Residue Inhibits the Binding of O_2 and NO at the Distal Heme Site of Cytochrome c'. *J. Am. Chem. Soc.* **2012,** 134, 1461-1463.

15. Antonyuk, S. V.; Rustage, N.; Petersen, C. A.; Arnst, J. L.; Heyes, D. J.; Sharma, R.; Berry, N. G.; Scrutton, N. S.; Eady, R. R.; Andrew, C. R.; Hasnain, S. S., Carbon monoxide poisoning is prevented by the energy costs of conformational changes in gas-binding haemproteins. *Proc. Natl. Acad. Sci.* **2011,** 108, 15780-15785.

16. Kruglik, S. G.; Lambry, J. C.; Cianetti, S.; Martin, J. L.; Eady, R. R.; Andrew, C. R.; Negrerie, M., Molecular Basis for Nitric Oxide Dynamics and Affinity with Alcaligenes xylosoxidans Cytochrome c'. *J. Biol. Chem.* **2007,** 282, 5053-5062.

17. Yoo, B.; Lamarre, I.; Martin, J. L.; Andrew, C. R.; Negrerie, M., Picosecond Binding of the His Ligand to Four-Coordinate Heme in Cytochrome c': A One-Way Gate for Releasing Proximal NO. *J. Am. Chem. Soc.* **2013,** 135, 3248-3254.

18. Andrew, C. R.; Rodgers, K. R.; Eady, R. R., A Novel Kinetic Trap for NO Release from Cytochrome c': A Possible Mechanism for NO Release from Activated Soluble Guanylate Cyclase. *J. Am. Chem. Soc.* **2003,** 125, 9548-9549.

19. Barbieri, S.; Murphy, L. M.; Sawers, R. G.; Eady, R. R.; Hasnain, S. S., Modulation of NO binding to cytochrome c' by distal and proximal haem pocket residues. *J. Biol. Inorg. Chem.* **2008,** 13, 531-540.

20. Cusanovich, M. A.; Tedro, S. M.; Kamen, M. D., Pseudomonas denitrificans Cytochrome cc'. *Arch. Biochem. Biophys.* **1970,** 141, 557-570.

21. Greetham, G. M.; Burgos, P.; Cao, Q.; Clark, I. P.; Codd, P. S.; Farrow, R. C.; George, M. W.; Kogimtzis, M.; Matousek, P.; Parker, A. W.; Pollard, M. R.; Robinson, D. A.; Xin, Z. J.; Towrie, M., ULTRA: A Unique Instrument for Time-Resolved Spectroscopy. *Appl. Spectrosc.* **2010,** 64, (12), 1311-9.

22. Jones, A. R.; Russell, H. J.; Greetham, G. M.; Towrie, M.; Hay, S.; Scrutton, N. S., Ultrafast Infrared Spectra Fingerprints of Coenzyme B12 and Related Cobalamins. *J. Phys. Chem. A* **2012,** 116, 5586-5594.

23. Lin-Vien, D.; Colthup, N. B.; Fateley, W. G.; Grasselli, J. G., *The Handbook of Infrared and Raman Characteristic Frequencies of Organic Molecules*. Academic Press: San Diego, 1991.

24. Hellwig, P.; Grzybek, S.; Behr, J.; Ludwig, B.; Michel, H.; Mantele, W., Electrochemical and Ultraviolet/Visible/Infrared Spectroscopic Analysis of Heme a and a3 Redox Reactions in Cytochrome c Oxidase from Paracoccus denitrificans: Separation of Heme a and a3 Contributions and Assignment of Vibrational Modes. *Biochemistry* **1999,** 38, 1685-1694.

25. Zemojtel, T.; Rini, M.; Heyne, K.; Dandekar, T.; Nibbering, E. T. J.; Kozlowski, P. M., NO-Bound Myoglobin: Structural Diversity and Dynamics of the NO Ligand. *J. Am. Chem. Soc.* **2004,** 126, 1930-1931.

Dynamics of Chemical and Photochemical Reactions in Solution

Contact *A.Orr-Ewing@bristol.ac.uk, Mike.Ashfold@bristol.ac.uk*

Greg T. Dunning, Fawzi Abou-Chahine, Stephanie J. Harris, Daniel Murdock, Michael P. Grubb, Michael N.R. Ashfold, David R. Glowacki, Jeremy N. Harvey and Andrew J. Orr-Ewing

School of Chemistry, University of Bristol, Cantock's Close, Bristol, BS8 1TS, UK

Stuart J. Greaves

School of Engineering and Physical Sciences, Heriot-Watt University, Edinburgh, EH14 4AS, UK

Gregory M. Greetham, Ian P. Clark and Mike Towrie

Central Laser Facility, STFC, Rutherford Appleton Laboratory, Didcot, Oxfordshire, OX110QX

Introduction

The liquid phase provides a medium for many important synthetic and biological chemical reactions, yet the role played by the solvent is often poorly defined. In a liquid environment, collisions between reactants and the solvent molecules occur with typical intervals of ~100 fs that are competitive with the timescales for chemical reaction. These solvent collisions influence the energy flow over the course of the reaction, equilibrate the products with the solvent bath, and may modify both the energy landscape over which reaction occurs and the motions of the reacting atoms and molecules (the reaction dynamics). Our investigations seek to draw detailed comparisons between the dynamics of chemical reactions observed under isolated conditions in the gas phase, and those exhibited by the same reactions in liquids. Such contrasts provide robust evidence for the influence the solvent exerts on chemical mechanisms. The experimental studies carried out using the ULTRA Facility address both bimolecular reactions [1-3] and unimolecular photodissociation processes [4,5], and both strands are reinforced by computational calculations of the energy landscapes and chemical dynamics [6]. The broad conclusion drawn from the evidence acquired to date is that, for many organic solvents such as acetonitrile, dichloromethane, and hexane/cyclohexane, the prompt dynamics in solution are remarkably similar to those observed in the gas phase. However, the liquid environment further influences the dynamics on timescales longer than the first few picoseconds by processes not possible under isolated collision conditions, including solvent caging, geminate recombination (including isomerization), vibrational coupling and electronic quenching. Such processes are not only observed but their rates are quantified, and detailed mechanisms unraveled through a combination of ultrafast transient absorption spectroscopy measurements in the ultraviolet (UV) and infra-red (IR) regions, and complementary theoretical calculations. The following two sections illustrate some of the most recent insights from this work.

Bimolecular Reaction Dynamics

Our prior time-resolved IR absorption studies of exothermic reactions of CN radicals with cyclohexane [1] and tetrahydrofuran [2], and of Cl atoms with 2,3-dimethylbut-2-ene [3] demonstrated formation of vibrationally excited products, consistent with an early transition state, and their subsequent relaxation by coupling to the solvent bath. Extension of this work to the reactions:

$$F + CD_3CN \rightarrow DF + CD_2CN \qquad \Delta_rH = -158 \text{ kJ mol}^{-1} \qquad (1)$$

$$F + CD_2Cl_2 \rightarrow DF + CDCl_2 \qquad \Delta_rH = -151 \text{ kJ mol}^{-1} \qquad (2)$$

indicates that the DF is also formed vibrationally hot, but that it relaxes to the vibrational ground state on timescales shorter than 20 ps. Figure 1 shows a single time step in a computer simulation of reaction (1), which provides important insights for interpretation of the experimental data. The analysis of time-resolved IR spectra is complicated by the considerable broadening of the DF vibrational bands in solution, as is evident in figure 2, interference from overlapping solvent bands, and the substantial shifts in frequency of the DF vibrational bands with change from free DF molecules to hydrogen bonded complexes with radical co-products or solvent molecules. Evolution of the shapes of the absorption bands evident in figure 2 is attributed to a combination of vibrational relaxation and changes in solvation environment.

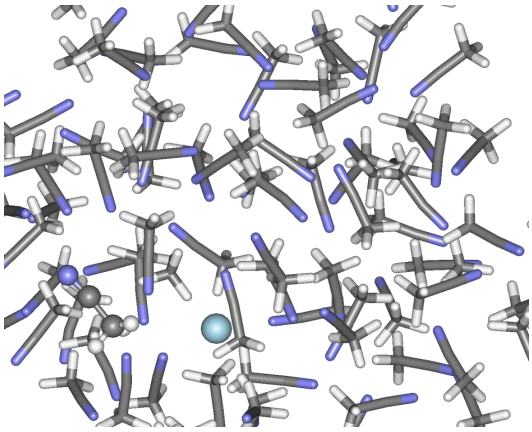

Figure 1: Snapshot from a computer simulation of the reaction of F atoms with solvent CD_3CN.

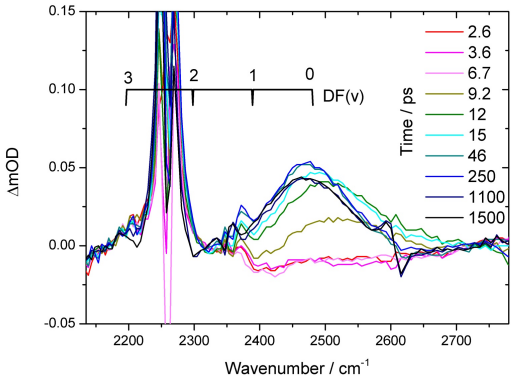

Figure 2: Selected time-resolved IR spectra for the DF products of reactions of F-atoms with liquid CD_3CN. The inset key shows the time delays between initiation of reaction and spectroscopic observation of products with a broadband, ultrafast IR laser pulse. The broad feature centred at ~2480 cm^{-1} is DF absorption, and the sharper structures from 2200-2300 cm^{-1} result from interference by solvent CD_3CN bands. The comb indicates where hot bands from absorption by vibrationally excited DF are expected to be centred.

Analysis of the time-resolved IR spectral intensities and band shapes indicates that the reaction in solution produces DF in vibrational levels up to v=2 or 3 for reactions (1) and (2). These

reactions are known to form DF with still greater vibrational excitation in the gas phase (up to the limit imposed by the reaction exothermicity), indicating that the solvent partially (but not completely) damps the energy flow to the newly forming D-F bond. This conclusion is consistent with our prior results for CN radical and Cl atom reactions in solution, and a general picture is now emerging about how solvent friction influences the dynamics of these exothermic H-atom (or D-atom) transfer reactions.

Photodissociation Dynamics

Previous ultrafast UV pump/UV-vis transient absorption (TA) studies of the photodissociation of *p*-methylthiophenol (*p*-MePhSH) in ethanol solution confirmed that the dominant gas phase process (prompt S–H bond fission) following population of the $1^1\pi\sigma^*(S_2)$ excited state persists in solution also [7]. Access to the ULTRA Facility allowed more detailed study of this (and related) UV photolyses, using time-resolved IR absorption methods to follow the evolving populations of the ground (S_0) state parent molecule, of the radical products and alternative recombination products. Figure 3 shows illustrative data following 267 nm photolysis of *p*-MePhSH and its close relative *p*-methylthioanisole (*p*-MePhSMe) in CD_3CN solvent. Analysis of the former data confirms prompt depletion of the ground (S_0) state parent and formation of *p*-MePhS(X) products within the effective experimental response time (~1 ps), but also allows us to follow the vibrational cooling of these radicals (with time constant τ~8.5 ps), and to determine that ~30% of these radicals undergo geminate recombination on a longer (~150 ps) timescale. Two recombination routes are identified. One involves S–H bond reformation, restoring some of the S_0 population and thereby reducing the parent bleach signal. Complementary theory shows that the other route, which reveals itself through the appearance of a new feature at ~1625 cm^{-1}, involves H atom addition to the ring, yielding a thioquinone-like structure [4].

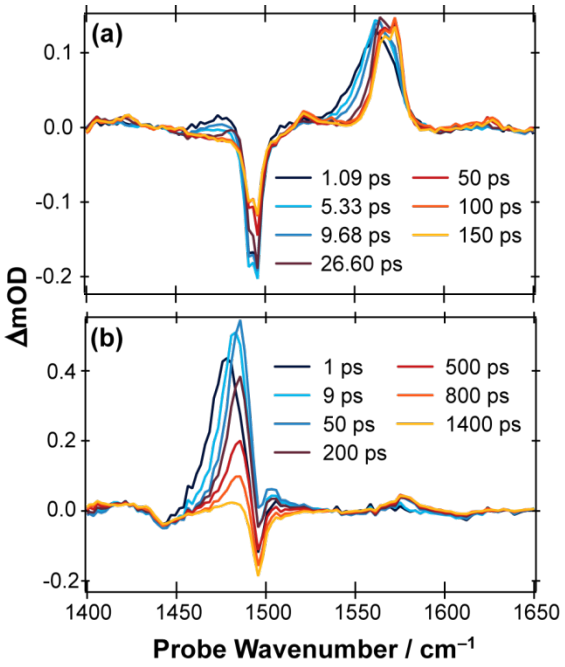

Figure 3: Time-resolved IR absorption spectra measured at different time delays following 267 nm photoexcitation of (a) *p*-MePhSH and (b) *p*-MePhSMe in CD_3CN. The ~1495 cm^{-1} and ~1570 cm^{-1} peaks in (a) are signatures of, respectively, the (depleted) S_0 parent population and the newly formed *p*-MePhS(X) radical; the thioquinone-like adduct reveals itself through the weak feature at ~1625 cm^{-1}. (b) is dominated by a broad absorption centred at ~1485 cm^{-1} attributable to *p*-MePhSMe(S_1) molecules, some fraction of which decay to yield the same ~1570 cm^{-1} *p*-MePhS radical feature as in (a).

267 nm photoexcitation of *p*-MePhSMe populates the $1^1\pi\pi^*(S_1)$ state. The broad peak at ~1485 cm^{-1} in fig. 3(b) is the transient IR absorption of this population. With increasing time, this feature narrows and shifts to higher wavenumber (reflecting the vibrational relaxation of the S_1 population) and declines in intensity, while another feature develops at ~1570 cm^{-1}. As in fig. 3(a), the latter feature is attributable to *p*-MePhS radicals, and a full analysis of the time evolving band shapes and intensities reveals two contributions to the S_1 population loss – S–Me bond fission following radiationless transfer via a conical intersection (CI) to the dissociative $1^1\pi\sigma^*(S_2)$ potential, and internal conversion to the S_0 state, with relative probabilities that are sensitive to the vibrational energy content in the S_1 parent [4]. Both molecules show similar photochemical behaviours in cyclohexane solution also [5]; in all cases, we find that insights gained from studying the corresponding photolysis in the gas phase provides a valuable starting point for describing the solution phase dynamics.

Photoexciting gas phase phenol molecules to their $1^1\pi\pi^*(S_1)$ state leads to O–H bond fission, on a *nanosecond* timescale, by tunneling through the substantial barrier under a conical intersection linking the S_1 and $1^1\pi\sigma^*(S_2)$ potential energy surfaces. Phenol molecules in solution suffer thousands of collisions on this timescale, yet IR and UV-vis TA studies following 267 nm excitation of phenol in cyclohexane solution show this same fragmentation process persisting in the condensed phase [5]. Analogy with the thioanisole study encouraged exploration of the photolysis of ethers in solution. First proving studies following 267 nm photo-excitation to the S_1 state of allyl phenyl ether in cyclohexane solution confirm RO–allyl bond fission (the first step in a photo-Claisen rearrangement) on a ~90 ps timescale, and subsequent recombination yielding an allyl substituted cyclohexadienone.

Conclusions

Ultrafast time-resolved IR absorption spectroscopy, carried out using the ULTRA Facility, is allowing study of the formation of products of both bimolecular reactions and unimolecular photofragmentation processes in solution in real time. Through collisions on a ~100 fs timescale and through intermolecular interactions, the liquid environment exerts a perturbation on the molecular motions in both cases, yet the early time dynamics are remarkably similar to those observed under isolated conditions in the gas phase. However, subtle differences between the chemical dynamics in these two environments are providing important new insights into the modification of reaction mechanisms by a liquid solvent.

Acknowledgements

The Bristol group gratefully acknowledges funding from the EPSRC Programme Grant EP/G00224X and the ERC Advanced Grant 290966 CAPRI. S.J.G. thanks the EPSRC for a Career Acceleration Fellowship (EP/J002534/1). The ULTRA laser complex at the Central Laser Facility, Rutherford Appleton Laboratory is funded by STFC and BBSRC (STFC Facility Grant ST/501784).

References

1. S.J. Greaves *et al.* Science, **331**, 1423 (2011).
2. R.A. Rose *et al.*, PCCP **14**, 10424 (2012).
3. F. Abou-Chahine *et al.*, Chem. Sci. **4**, 226 (2013).
4. D. Murdock *et al.*, J. Phys. Chem. Lett. **3**, 3715 (2012).
5. S.J. Harris *et al.*, PCCP **15**, 6567 (2013).
6. D.R. Glowacki *et al.*, Nature Chem. **3**, 850 (2011).
7. Y. Zhang *et al.*, Farad. Disc. **157**, 141 (2012).

Time-resolved vibrational spectroscopy of Trolox C photoionization

Contact *r.h.bisby@salford.ac.uk*

R H Bisby
University of Salford

G M Greetham
LSF, Central Laser Facility

A W Parker
LSF, Central Laser Facility

M Towrie
LSF, Central Laser Facility

K M Scherer
LSF, Central Laser Facility

Introduction

Life in an oxygen-containing environment leads to oxidative stress that is potentially damaging to biomolecules and cellular processes. An important example is the peroxidation of polyunsaturated acyl chains in lipids that might eventually lead to atherosclerosis [1]. Such damage is limited by a range of protective mechanisms, including vitamin E that functions as a chain-breaking antioxidant in cell membranes and lipoproteins [2]. Much interest has focused on the mechanism of this reaction that may be viewed as a hydrogen atom transfer from the phenolic group of vitamin E to the chain-propagating lipid peroxyl radical. However some evidence suggests concerted electron and proton transfer as an alternative mechanism [3, 4]. In order to understand the process of electron loss from vitamin E we have studied the photoionization initiated by nanosecond [5] and picosecond photolysis [6]. In our current studies we have used femtosecond stimulated Raman spectroscopy (FSRS) and time-resolved infrared (FTIR) spectroscopy to observe the kinetics of photoionization of Trolox C (T-OH, a water soluble vitamin E analogue). In combination with an actinic pulse to prepare the intermediate of interest, FSRS uses a picosecond Raman pump pulse in combination with a femtosecond whitelight continuum to probe the reaction progress, and offers superior temporal and spectral resolution compared with time-resolved resonance Raman (TR^3) spectroscopy [7].

Transient Absorption Spectra

Transient absorption spectra from photolysis with 200 fs pulses at 266 nm of Trolox C in D_2O solution are shown in Figure 1. The main species present at 1 ps after the actinic pulse has an absorption at *ca.* 550 nm which is believed to be the excited state.

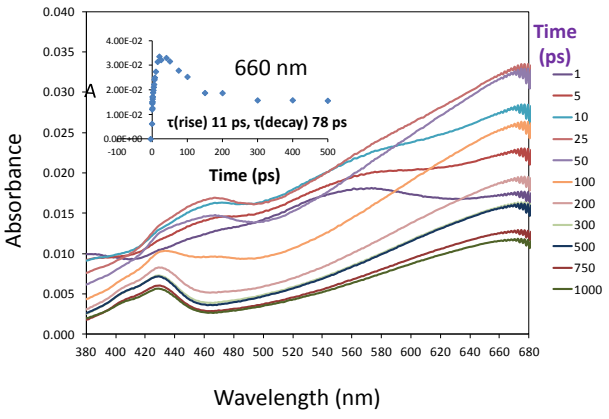

Figure 1 – Transient absorption spectra measured at the indicated times after 266 nm photolysis of Trolox C in D_2O at pH 7. The **inset** shows the formation and decay of the transient at 660 nm.

By 25 ps after the actinic pulse new transients are observed at > 650 nm, belonging to the hydrated electron, and at 450 nm due the radical cation of Trolox C:-

$$\text{T-OH} + h\nu \rightarrow \text{T-OH}^{+\bullet} + e^-_{aq}$$

Between 50 and 1000 ps the hydrated electron partially decays to leave a fraction seen in previous nanosecond experiments [8]. The 450 nm absorption also decays such that by 100 ps it is replaced by the spectrum of the neutral Trolox C radical:-

$$\text{T-OH}^{+\bullet} \rightarrow \text{T-OH}^{\bullet} + H^+$$

Although the essential signatures of the species evolving on the picosecond timescale are apparent in the transient absorption spectra, their spectra overlap considerably making kinetic interpretation more difficult. Consequently the reactions were investigated using time-resolved vibrational spectroscopy.

Femtosecond Stimulated Raman Spectroscopy (FSRS)

FSRS spectra from photoionization of Trolox C in neutral aqueous solutions are shown in Figure 2.

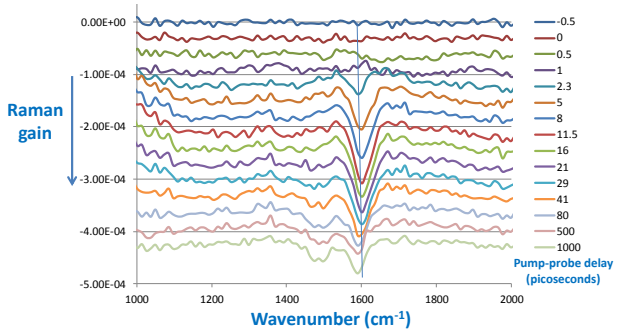

Figure 2 – Femtosecond stimulated Raman spectra of radicals formed by photolysis of Trolox C in neutral H_2O solution, obtained using a 266 nm actinic pulse and 450 nm Raman pump pulse.

At early times the main feature of these spectra is the band at 1607 cm^{-1} previously observed by nanosecond TR^3 in very acidic solutions and assigned to the ν_{8a} C=C ring stretching mode of the radical cation [5]. This band grows in over the initial 10 ps period and is then replaced by two bands at 1494 cm^{-1} and 1596 cm^{-1} which are the C-O ν_{7a} and C=C ν_{8a} ring modes of the Trolox C neutral radical. The kinetics for growth and decay of the radical cation band are shown in Figure 3 and indicate that the band grows in with a lifetime of 7.6 ps and then decays with a lifetime of 42.6 ps. In D_2O solution both of these lifetimes show a kinetic isotope effect and increase by a factor of 2 to 3, indicating the involvement of a proton (or deuteron) in these processes. The decay process has a rate that corresponds to the decay of the hydrated electron and indicates that the two processes are linked. In effect the Trolox C radical cation is a strong acid and the fast deprotonation provides a proton for reaction with a nearby hydrated electron within an ion pair.

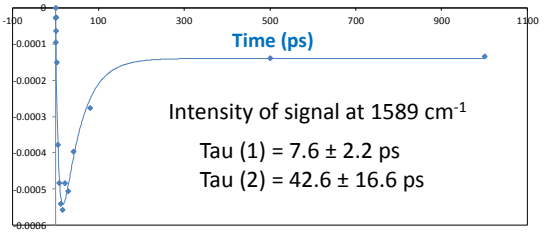

Figure 3 – Kinetics for formation and decay of the intensity of the neutral radical signal in Figure 2.

Once the ion pair has separated the hydrated electron assumes the normal lifetime of in the microsecond regime in neutral water, thereby accounting for the "permanent" residual absorption at > 650 nm in the sub-nanosecond timescale.

Picosecond Time-Resolved Infrared (TRIR) Spectra

Complementary picosecond TRIR spectra for vitamin E and Trolox C were measured in methanol-d_4 and D_2O solutions. Figure 4 shows TRIR spectra for vitamin E in MeOD together with the ground state FTIR spectrum. At early times there are

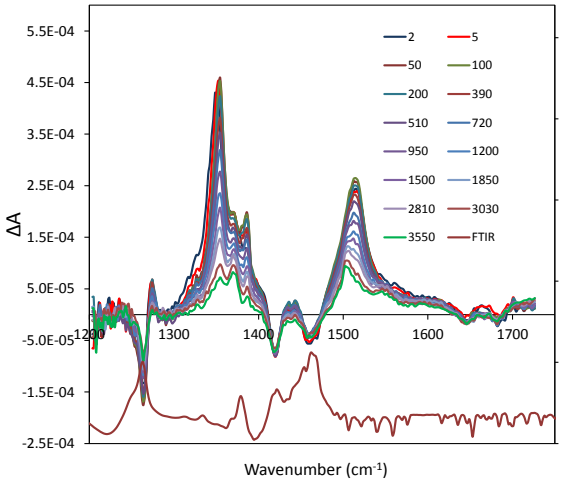

Figure 4 – TRIR spectra recorded from a solution of vitamin E (60 mM) in MeOD-d_4 at the indicated times (picoseconds) between 266nm pump (1 μJ) and probe pulses. The FTIR spectrum is shown below.

major transient absorptions at 1350 and 1514 cm^{-1}, the former showing significant vibrational relaxation during the initial 10 ps period. These are assigned to the excited state since the lifetimes of these two transients are 1.2 ns and correspond to the fluorescence lifetime of vitamin E in methanol [9]. It is noteworthy that the transient at 1514 cm^{-1} decays to reveal a more stable underlying transient at 1503 cm^{-1} that corresponds to the C-O ν_{7a} vibrational mode of the neutral tocopheroxyl radical. Also the bleaching of the ground state bands remains on this timescale, and the results are entirely consistent with homolytic photolysis of the phenolic –OH bond of vitamin E in this solvent [10].

Similar data for the photolysis of Trolox C in D_2O solution is shown in Figure 5. In contrast the excited state transients are very short-lived (τ ~ 50 ps), consistent with the much lower fluorescence quantum yield for Trolox in aqueous solution. Compared with the spectra for vitamin E, the additional bleach of the carboxylate absoprtion in Trolox C is observed at 1575 cm^{-1}. This recovers only partially as the radicals that are formed have longer lifetimes. No corresponding positive band for the carboxylate group in the excited state or radical products is observed, probably because this has a lower bond order and smaller extinction coefficient compared with the parent carbonyl group. Another new transient absorption is also observed at 1609 cm^{-1}. This has a lifetime of 67 ± 11 ps that is similar to the lifetime of the radical cation in D_2O observed by FSRS and occurs in a similar spectral position to that from another water soluble vitamin E analogue measured in nanosecond experiments [8]. As in the spectra shown in

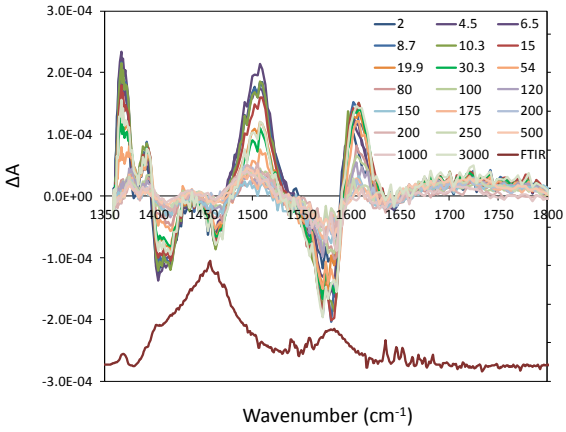

Figure 5 – TRIR spectra from 266 nm photolysis of Trolox C (7.5 mM) in D_2O solution at pD 7.

Figure 4 for vitamin E in MeOD, the TRIR spectra from photolysis of Trolox C in D_2O also reveal a small residual band at about 1490 cm^{-1} that corresponds to the neutral radical species.

Conclusions

Time-resolved vibrational spectroscopy offers a detailed insight into the kinetics of radical formation following photolysis of vitamin E and analogues. It shows that in neutral solutions the radical cation of Trolox C is a strong acid that rapidly loses a proton on the picosecond timescale. In the oxidation of vitamin E by peroxyl radical, this result suggests that electron transfer is very likely to involve a concerted proton loss and there is no need to consider a mechanism such as sequential proton loss/electron transfer as has recently been proposed [11].

Acknowledgements

We thank STFC and the University of Salford for provision of the studentship to KMS and STFC for access to facilities. We also thank Dr P. Kukura (University of Oxford) for advice on FSRS.

References

1. H Esterbauer *et al* (1993) *Br. Med. Bull*., **49**: 566-576.
2. M G Traber *et al* (2007) *Free Radic. Biol. Med*., **43**: 4-15.
3. S Nagaoka *et al* (1992) *J. Phys. Chem.*, **96:** 2754-2761.
4. Y Kohno *et al* (2011) *J. Phys. Chem. B,* **8**: 9880-9888.
5. A W Parker & R H Bisby (1993) *J. Chem. Soc. Faraday Trans*., **89**: 2873-2878.
6. M Towrie *et al* (1991) *Laser Chem*., **19:** 153-159.
7. P Kukura *et al* (2007) *Ann. Rev. Phys. Chem.*, **58:** 461-488.
8. R H Bisby & A W Parker (1991) *FEBS Lett.*, 290: 205-208.
9. R H Bisby & S Ahmed (1989) Free Radic. Biol. Med., 6: 231-239.
10. Y Zhang *et al* (2011) J. Phys. Chem. A , 115: 8242-8247.
11. M E Alberto *et al* (2013) Phys. Chem. Chem. Phys., 15: 4642-4650.

Intra- and Intermolecular Photoinduced Electron Transfer Acceleration in Azurin Mutants Labeled with a Re-carbonyl-diimine Chromophore

Contact *a.vlcek@qmul.ac.uk*

A. Vlček

Queen Mary, University of London
Mile End Road, E1 4NS London, UK

M. Towrie

STFC, Rutherford Appleton Laboratory
Didcot, Oxfordshire OX11 0QX, UK

H.B. Gray

Beckman Institute, California Institute of Technology
Pasadena, CA 91125, USA

J. Winkler

J. Beckman Institute, California Institute of Technology
Pasadena, CA 91125, USA

Introduction

Re carbonyl-diimine complexes become strong photoxidants upon excitation to their metal to ligand charge transfer (^{3}MLCT) state, whereby an electron is excited from a predominantly Re-based to a diimine-localized molecular orbital.[1] Laser-pulse excitation of proteins with covalently attached Re chromophores can thus trigger electron transfer (ET) from reducing centers (*e.g.* Cu^I in azurins), whose rate, however, decays exponentially with the distance between the redox sites. Herein we describe (ultra)fast photoinduced electron transfer in two Re-labeled azurin mutants that contain a tryptophan residue in a close vicinity of the chromophore. The kinetics and mechanism were revealed by a combination of time-resolved spectroscopic experiments, namely emission from the ^{3}MLCT Re excited state, 632.8 nm transient absorption due to oxidized Cu^{II}, and time-resolved IR spectroscopy (TRIR) in the ν(CO) spectral region, measured on both the PIRATE and ULTRA instruments at CLF.

Intramolecular ET: Re124W122AzCu

This azurin mutant contains a $Re^I(CO)_3$(dmp) chromophore bound to an imidazole side chain of H124 residue (dmp = 4,7-dimethyl-1,10-phenanthroline). The indole group of W122 is in contact (3.8 Å) with the dmp ligand and their aromatic rings are nearly parallel.[2]

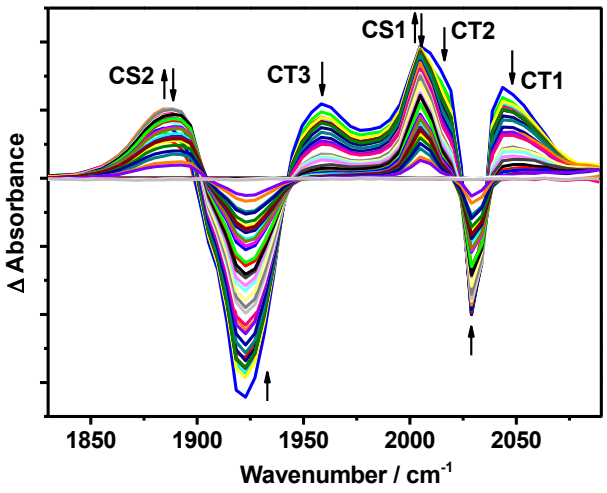

Figure 1. TRIR spectra of $Re124W122AzCu^I$ measured over the time interval 2-4000 ns. (CS signal appears in ≤1 ps)

TRIR spectra (Figure 1) show decaying up-shifted bands due to the ^{3}MLCT state (CT) $Re^{II}(CO)_3(dmp^{-})$ as well as down-shifted bands attributable to the CS state $Re^I(CO)_3(dmp^{\cdot-})$, in which the excited Re chromophore was reduced by the proximal tryptophan. (For assignment, see ref.[3]) The CS bands first grow with <1ps, ps, and ~2 ns lifetimes and than decay (6 μs). The Cu^{II} absorption rises during the first 50 ns and then decays with a 3.1 μs lifetime.[2] Detailed kinetics analysis of emission, TA, and TRIR data revealed the mechanism and elementary rate constants summarized in Scheme 1.[2]

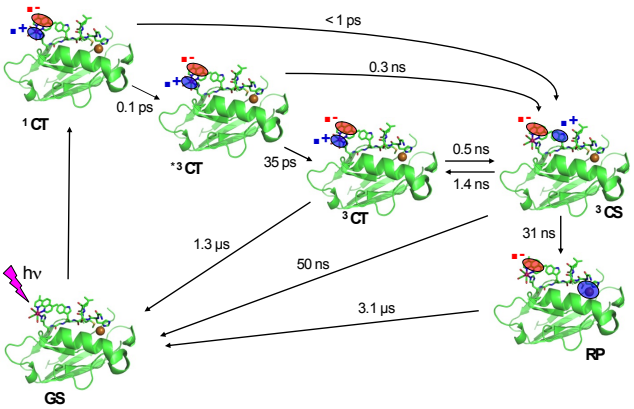

Scheme 1. Photoinduced electron transfer in $Re124W122AzCu^I$

The mechanism can be briefly described: Optical excitation of the Re label produces a ^{1}MLCT state that undergoes several ultrafast relaxation steps to the ^{3}MLCT state, which establishes an equilibrium with the CS state, by a ns ET $Re^{II}(dmp^{\cdot-})W122 \leftrightarrow Re^I(dmp^{\cdot-})W122^{\cdot+}$. This is the crucial step that stores part of the excitation energy in the form of the long-lived ^{3}MLCT state and "feeds" the next ~30 ns redox step $Re^I(dmp^{\cdot-})W122^{\cdot+} \leftarrow Cu^I$, producing the redox product (RP) $Re^I(dmp^{\cdot-})W122AzCu^{II}$. The photocycle is completed by 3.1 μs back electron transfer. The crucial point is that the $^*Re \leftarrow Cu^I$ ET over 19.4 Å is accelerated by electron hopping through the tryptophan intermediate W122. Quantum chemical calculations have revealed[4] a strong electronic interaction between the dmp and W122-indole rings in the ^{3}MLCT state, preceding the ET proper. This coupling seems to be crucial for the (ultra)fast ET and implies that the Re^I(dmp)W122 moiety can be regarded as a single photoactive unit.

Intermolecular ET: Re126W122AzCu

To test the above hypothesis about the crucial role of the Re^I(dmp)-W122-indole coupling, we have designed and prepared[5] another mutant where the Re chromophore is bound at position 126, that is 2 aminoacid residues farther from W122 than in Re124W122AzCu. The 10 Å intramolecular distance between the dmp and indole effectively prevents any direct interaction. Despite this, TRIR spectra (Figure 2) show very similar behavior as that found for $Re124W122AzCu^I$, including

the (sub)ps CS formation. On the ns scale, the CS formation is slightly slower than for the 124 mutant and the CS/RP yield is smaller, as judged by the maximum intensity of CS/RP2 relative to the initial CT3 intensity. TA at 632.8 nm shows Cu^{II} formation in ≤50 ns, but in a lower yield.

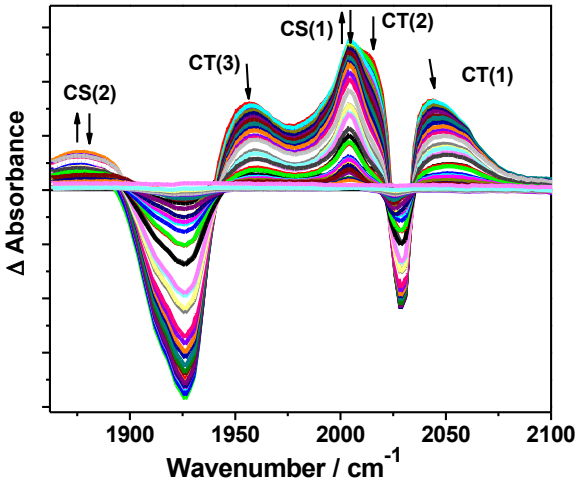

Figure 2. TRIR spectra of Re124W122AzCu^{I} measured over the time interval 2 ns-50 μs. (CS signal appears in ≤1 ps)

Solution of this puzzle emerged from the dependence of the Cu^{II} yield and of the kinetics on the concentration, indicating that the photocycle occurs in a dimer, whose presence in solution was indeed confirmed by mass spectrometry.[5] The crystal structure of Re126W122AzCu^{II} shows that intermolecular distances between the redox-active units are much shorter than the intramolecular ones. For example, the intermolecular dmp-indole distance is 3.5 Å, providing for a good electronic coupling across a hydrophobic protein-protein interface. The reaction mechanism is shown in Scheme 2. It is an intermolecular counterpart of the intramolecular hopping scheme established for Re124W122AzCu. The crucial CT↔CS equilibrium now involves a ns interfacial electron transfer. Cu^{I} oxidation by $W122^{\cdot+}$ is intramolecular, following the same pathways as in Re124W122AzCu. The back electron transfer Cu^{II}←$Re(dmp^{\cdot-})$ occurs with 220 ns and 6 μs lifetimes that have been explained by assuming an equilibrium between two redox product forms, reactive and unreactive.[5]

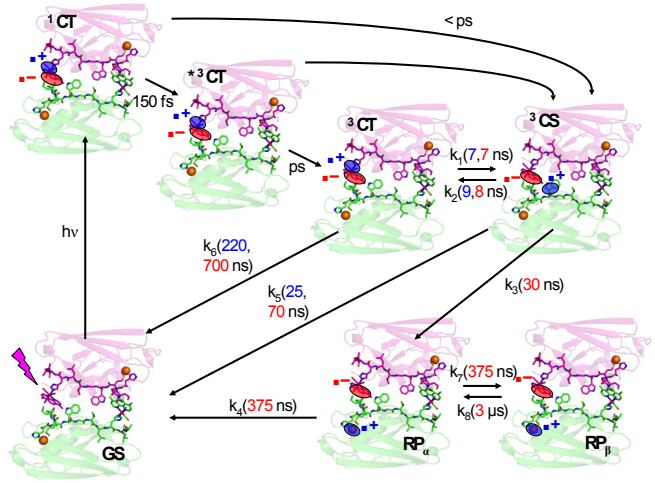

Scheme 2. Photoinduced electron transfer in Re126W122AzCu^{I}

Conclusions

Charged separation over long distances can be dramatically accelerated by inserting a tryptophan residue into the ET pathway. In the case of a Re(I) tricarbonyl-diimine labeled azurins, the primary electron transfer takes place in several steps on a time scale ranging from (sub)ps to few ns, provided that the diimine and indole rings are in a close proximity. Such interaction and, hence (ultra)fast electron transfer can occur either intra- or intermolecularly, across a protein-protein interface. Time-resolved IR spectral measurements over a broade time range (ps-μs) emerge as a powerful technique to study electron transfer in metallolabeled azurins, providing structural and kinetics information on the reacting excited state, the intermediate and product states, as well as on the ground-state recovery.

Acknowledgements

C. Shih, K. Takematsu, H. Williamson (Caltech), A.M. Blanco-Rodriguez (QMUL), S. Záliš, H. Kvapilová (J.Heyrovský Inst. Prague), I.P. Clark (STFC-RAL), and L. Sokolová (Goethe University, Frankfurt) are thanked for their important contibutions. The research was financed by NIH, NSF, STFC, and QMUL.

References

1. Vlček, A., Jr. *Top. Organomet. Chem.* **2010**, *29*, 73-114.

2. Shih, C.; Museth, A. K.; Abrahamsson, M.; Blanco-Rodriguez, A. M.; Di Bilio, A. J.; Sudhamsu, J.; Crane, B. R.; Ronayne, K. L.; Towrie, M.; Vlček, A., Jr.; Richards, J. H.; Winkler, J. R.; Gray, H. B. *Science* **2008**, *320*, 1760-1762.

3. Blanco-Rodríguez, A. M.; Towrie, M.; Sýkora, J.; Záliš, S.; Vlček, A., Jr. *Inorg. Chem.* **2011**, *50*, 6122–6134.

4. Blanco-Rodríguez, A. M.; Di Bilio, A. J.; Shih, C.; Museth, A. K.; Clark, I. P.; Towrie, M.; Cannizzo, A.; Sudhamsu, J.; Crane, B. R.; Sýkora, J.; Winkler, J. R.; Gray, H. B.; Záliš, S.; Vlček, A., Jr. *Chem. Eur. J.* **2011**, *17*, 5350 – 5361.

5. Takematsu, K.; Williamson, H.; Blanco-Rodríguez, A. M.; Sokolová, L.; Nikolovski, P.; Kaiser, J. T.; Towrie, M.; Clark, I. P.; Vlček, A., Jr.; Winkler, J. R.; Gray, H. B. *J. Am. Chem. Soc., submitted*.